6984 *Biochemistry* **2010,** *49,* 6984–6991
DOI: 10.1021/bi100727y

BIOCHEMISTRY
including biophysical chemistry & molecular biology
Article

Volume Exclusion and Soft Interaction Effects on Protein Stability under Crowded Conditions[†]

Andrew C. Miklos,[‡] Conggang Li,[‡] Naima G. Sharaf,[‡] and Gary J. Pielak*[,‡,§,∥]

[‡]*Department of Chemistry,* [§]*Department of Biochemistry and Biophysics, and* [∥]*Lineberger Comprehensive Cancer Center, University of North Carolina, Chapel Hill, North Carolina 27599*

Received May 7, 2010; Revised Manuscript Received July 8, 2010

ABSTRACT: Most proteins function in nature under crowded conditions, and crowding can change protein properties. Quantification of crowding effects, however, is difficult because solutions containing hundreds of grams of macromolecules per liter often interfere with the observation of the protein being studied. Models for macromolecular crowding tend to focus on the steric effects of crowders, neglecting potential chemical interactions between the crowder and the test protein. Here, we report the first systematic, quantitative, residue-level study of crowding effects on the equilibrium stability of a globular protein. We used a system comprising poly(vinylpyrrolidone)s (PVPs) of varying molecular weights as crowding agents and chymotrypsin inhibitor 2 (CI2) as a small globular test protein. Stability was quantified with NMR-detected amide ^{1}H exchange. We analyzed the data in terms of hard particle exclusion, confinement, and soft interactions. For all crowded conditions, nearly every observed residue experiences a stabilizing effect. The exceptions are residues for which stabilities are unchanged. At a PVP concentration of 100 g/L, the data are consistent with theories of hard particle exclusion. At higher concentrations, the data are more consistent with confinement. The data show that the crowder also stabilizes the test protein by weakly binding its native state. We conclude that the role of native-state binding and other soft interactions needs to be seriously considered when applying both theory and experiment to studies of macromolecular crowding.

Studies in dilute solution have yielded essential information about the biophysical properties of globular proteins. The complex milieu inside cells can change these properties (*1*−*4*). Studying the nature and magnitude of these changes should improve our understanding of how proteins function in their native environments. Our experiments focus on NMR-based approaches that quantify the effects of macromolecular crowding on equilibrium protein stability. Here we examine stability as a function of both the concentration and the molecular weight of a synthetic polymer. Studies such as these can provide both evidence of the importance of crowding in biological systems and quantitative results useful for verifying and refining predictions of crowding effects (*5*).

Stability is the difference in free energy between the unfolded-state ensemble (U) and the native state (N) (*6*). When a protein goes from dilute to crowded conditions, a transfer free energy from dilute solution to crowded conditions must be considered for both states (Figure 1). The transfer results in a new standard state with a new free energy of opening, ΔG^{0*}_{op}, for each residue. These values reflect both local and global unfolding events, and the largest values reflect global protein stability, $\Delta G^{0*}_{N\rightarrow U}$ (*7*). These changes in stability can be quantified by using NMR spectroscopy.

NMR-detected amide proton exchange allows investigation of protein stability in a crowded environment without extrapolation of temperature or cosolute concentration (*8*). ^{15}N−^{1}H heteronuclear single-quantum correlation (HSQC)[1] experiments are used to detect exchange in ^{15}N-enriched proteins (*9*, *10*). Signals from the crowder do not interfere because the natural abundance of any ^{15}N in the crowder is only 0.37%. The nature of the HSQC experiment also provides residue-level specificity. Although most previous studies focused on global stability, the stabilities of locally unfolded conformations are also important in biological functions such as binding (*11*). We present an overview of the theory of amide proton exchange below. A comprehensive review is available (*12*).

Scheme 1 describes amide proton exchange in proteins (*13*). The closed state (cl) is the native state. A proton can exchange only for a deuteron in an open state (op). Two quantities need to be determined: k_{int}, the intrinsic first-order rate of exchange for an unstructured peptide, and k_{obs}, the first-order rate of exchange of the amide proton in the test protein. Values for k_{obs} are determined through amide proton exchange experiments, while dilute solution k_{int} values are calculated by using a computer program, *SPHERE* (http://www.fccc.edu/research/labs/roder/sphere/) (*14*, *15*). Assuming the protein is stable ($k_{cl} \gg k_{op}$) and k_{int} is much smaller than k_{op} (*13*), ΔG^{0*}_{op} can be determined by using the equation (*12*)

$$\Delta G^{0^*}_{op} = -RT \ln\left(\frac{k_{obs}}{k_{int}}\right)$$

Provided these assumptions are true under crowded conditions, NMR-detected amide ^{1}H exchange experiments can be used to

[†]This work was supported by the National Institutes of Health (5DP1OD783) and the National Science Foundation (MCB-051647).

*To whom correspondence should be addressed. Phone: (919) 966-3671. Fax: (919) 962-2388. E-mail: gary_pielak@unc.edu.

[1]Abbreviations: CI2, chymotrypsin inhibitor 2; HSQC, heteronuclear single-quantum correlation; PVP, poly(vinylpyrrolidone); TMAO, trimethylamine *N*-oxide.

 Published on Web 07/13/2010

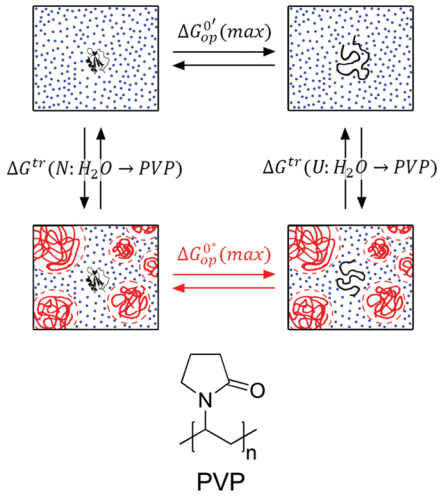

FIGURE 1: Diagram of protein stability relationships and the structure of PVP. $\Delta G^{0'}_{op}$(max) represents the dilute solution stability, and ΔG^{0*}_{op}(max) represents the stability under crowded conditions. ΔG^{tr} represents a transfer free energy between sets of solvent conditions.

obtain quantitative information about how crowding affects stability (*16*).

Two types of interactions, hard and soft, are used to explain the effects of crowding on ΔG^{0*}_{op}. Hard interactions, also known as volume exclusion, are the result of impenetrable crowding agents occupying solvent space, removing volume otherwise accessible to the protein (*17*). In this crowded environment, proteins are subjected to an entropic penalty if they have a large covolume with the crowder. The covolume can be considered the volume in which the center of mass of the protein cannot exist due to the presence of the crowder (*18*). Unfolded states have larger covolumes because of their larger radii of hydration compared to the native state (*19*). That is, volume exclusion can only increase protein stability and does so by destabilizing the denatured state. Next, we discuss two models of volume exclusion, hard particle exclusion and confinement (*17*, *20*).

Hard particle exclusion arises when macromolecular crowders act as independent particles. The change in stability caused by independent particles is expected to exhibit both a concentration and a molecular weight dependence (*21*). Confinement arises when the crowders create a cavity from which the protein cannot escape. The stability change in this instance is based on the size and shape of the cavity (*20*). For synthetic polymer crowders, a transition from hard particle crowding to confinement is expected above the polymer's overlap concentration (c^*), defined as the concentration above which the polymer molecules no longer act as individual particles. At this concentration, the solution moves from the dilute to semidilute regime, and polymers begin to become entangled (*22*).

Hard particle crowding and confinement, however, can only explain part of the observed effect, because these models assume that the crowding agent is inert. Few, if any, crowders exhibit such ideal behavior. Instead, crowding agents are expected to interact chemically with the protein (*23*). These soft chemical interactions must be considered.

Soft interactions affect both entropy and enthalpy and can be stabilizing or destabilizing. These interactions take into account the chemical nature of the molecules involved as opposed to treating them as hard spheres. We divide soft interactions into two types, nonspecific interactions and native-state interactions. Interactions involving urea, trimethylamine *N*-oxide (TMAO), and ligand binding provide three familiar examples of different types of soft interaction between proteins and small molecules.

Scheme 1: Reaction Diagram Describing Amide Proton Exchange with Associated Rate Constants, k_{cl}, k_{op}, and k_{int}

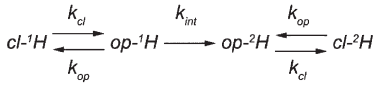

The effects of urea and TMAO have a common source, the protein backbone. These small molecules have nonspecific interactions with protein but have differing effects on stability. Urea has a favorable weak interaction with the protein backbone (*24*). As unfolded states expose more backbone to urea solutions than native states, urea destabilizes globular proteins. Conversely, the protein backbone interacts more favorably with H_2O than with TMAO, resulting in stabilization (*25*). These types of nonspecific interactions are commonly considered in studies involving proteins and cosolutes, but native-state interactions can also have an effect under crowded conditions.

Some small molecules stabilize proteins by specifically binding the native state, as seen in stabilization by ligand binding (*26*). Unlike nonspecific interactions, native-state interactions often lead to changes in the chemical environment for a specific region of the protein. Native-state binding is also possible for crowding agents, if the crowder has a favorable interaction with a specific protein structural element or region. Both volume exclusion and soft interactions play a role in crowding effects, and NMR can be used to assess soft interactions, even if they are weak.

The chemical shift of a nucleus reflects its local environment. Interactions between a crowding agent and the test protein can alter this environment, making even a NMR experiment as simple as chemical shift measurement a sensitive indicator of soft interactions. Chemical shift changes, however, can arise in several ways, from protein structure changes to binding to aggregation. We may be able to separate these contributions by assessing relaxation.

Chemical shift changes can suggest an interaction between the native state of the protein and the crowder. The product of R_1 and R_2, ^{15}N longitudinal and transverse relaxation rates, respectively, can provide more direct information about protein−crowder interactions. Kneller et al. showed that if a protein's rotational correlation time exceeds 6 ns, R_1R_2 is insensitive to viscosity and can be used to probe internal dynamics on the millisecond time scale (*27*). We realized this product was also useful for detecting soft interactions (*28*). We use R_1R_2 and changes in chemical shifts to interpret changes in ΔG^{0*}_{op} caused by crowding effects.

We use the I29A/I37H variant of chymotrypsin inhibitor 2 (CI2; Protein Data Bank entry 2CI2) as our test protein. It is a small (7.4 kDa) globular protein with two-state folding properties (*29*). CI2 (Figure 2) has a compact core containing its sole α-helix (Ser12−Lys24), two major β-sheet regions (Gln28−Val34 and Asp45−Asp52), an extended loop (Gly35−Ile44), and several turns. Dilute solution NMR-detected amide proton exchange experiments show that Lys11, Ile20, Leu21, Ile30, Val47, Leu49, Phe50, and Val51 are on the global unfolding path, which means they become exchange-competent only when the entire protein unfolds (*30*). These properties allow hydrogen exchange experiments to probe both local and global stabilities upon addition of a crowding agent.

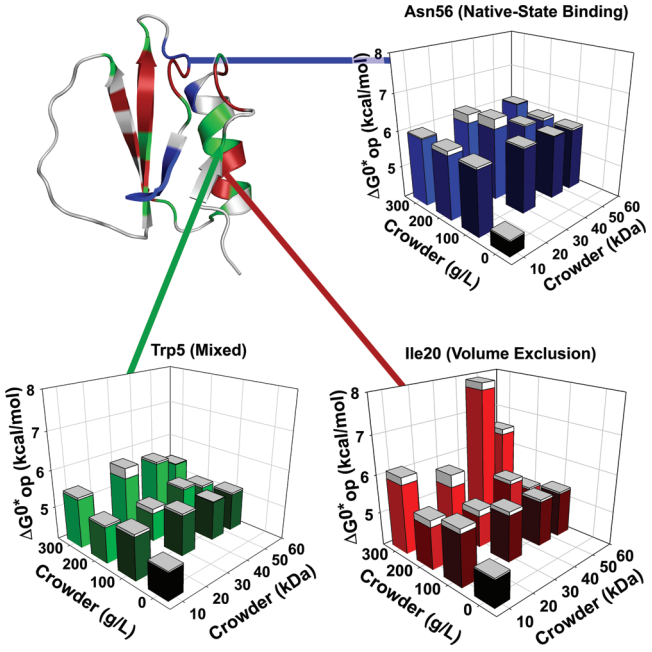

FIGURE 2: Structure of CI2 (Protein Data Bank entry 2CI2) and stability histograms. Residues are colored by stability trends. Red, blue, and green residues exhibit trends consistent with volume exclusion, native-state binding, and the mixed effect, respectively. Residues for which stabilities could not be measured are colored white. The mean ΔG^{0*}_{op} from three trials is plotted for Ile20, Trp5, and Asn56 as a function of PVP molecular weight and concentration (50 mM sodium acetate at pH 5.4 and 37 °C). The column caps represent the positive components of the standard errors. PyMol (*48*) was used to visualize the structure.

Table 1: Characterization of PVP-10, -29, -40, and -55

species	$\bar{M}_W$ (kDa)	$\bar{M}_N$ (kDa)	polydispersity	R_H (nm)	$\bar{\nu}_2$ (mL/g)	c^* (g/L)
PVP-10	10.2	5.1	2.0	2.2	0.807	470
PVP-29	29.7	13.0	2.28	4.9	0.806	120
PVP-40	44.9	13.4	3.35	5.6	—	130
PVP-55	55.0	12.5	4.38	6.7	0.798	90

We approach crowding systematically by varying the concentration and molecular weight of the crowding agent. Such reductionism is not feasible in the complex intracellular environment. For tight control of the concentration and molecular weight, we use the polymeric crowding agent poly(vinylpyrrolidone) (PVP) (*31*). PVP (Figure 1) has four advantageous properties. It is highly soluble (up to 300 g/L) and is available in several molecular weights (Table 1). The partial specific volume of PVP (0.80 mL/g) allows physiological volume occupancy to be obtained, and PVP interacts only weakly with proteins (*16*, *32*). Furthermore, this polymer can be studied both above and below c^* (Table 1), allowing us to explore both hard particle crowding and confinement, respectively. These properties make PVP an excellent choice for our experiments.

This system has been previously used in studies of macromolecular crowding effects. Ladurner and Fersht (*33*) used guanidinium chloride as a denaturant and intrinsic fluorescence as a detection method to assess the stability of CI2 in PVP. They found that CI2 is destabilized by 0.8 kcal/mol in 10 kDa PVP at 50 g/L. In contrast, Charlton et al. (*16*) used NMR-detected amide proton exchange to determine the effects of 40 kDa PVP at 300 g/L on CI2 stability and found a maximal stabilization of 3 kcal/mol. The apparent difference between these two results arises from the differences in the two approaches.

Detection methods such as fluorescence and circular dichroism (CD) spectroscopies allow determination of stability through the observation of structure. These techniques probe global stability. NMR-detected amide proton exchange experiments yield comparable global stabilities (*16*). NMR experiments, however, allow residue level determination of stability, providing a tool to study both global and local unfolding. These local unfolding events can often be as important as global events, and NMR is the only technique that can probe these effects throughout the protein in a single experiment. Most importantly, fluorescence and CD detection require perturbation of the system, whether by temperature changes or by addition of a denaturant for detecting folding or unfolding. NMR-detected amide proton exchange does not have these constraints and allows determination of stability without perturbing the system. Components of the system that react to changes in temperature or addition of denaturants can affect analysis. Denaturant-induced perturbations are especially important in crowding experiments, as the temperature and denaturant sensitive components exist at concentrations of ≥100 g/L.

The difference between the two results (*16*, *33*) can be explained in terms of denaturant-induced perturbations. It has been shown that guanidinium salts and urea alter the properties of PVP (*34*), suggesting that the two results cannot be compared. In essence, the CI2/PVP/guanidinium chloride system is different from the PVP/CI2 system. For this reason, native-state hydrogen exchange (*35*), which requires solutions containing both PVP and urea, was not used. Instead, NMR-detected amide proton exchange was performed without the addition of denaturants, as a function of PVP molecular weight and concentration.

The data obtained by Charlton et al. (*16*) showed the feasibility of using NMR-detected amide proton exchange to assess the effects of crowding on protein stability but were inadequate for the detection of the nuances of concentration and molecular weight dependencies. The results presented here quadruple the number of observations made previously (*16*). These new data allow the determination of concentration-dependent stability trends and molecular weight-dependent trends. The data also reveal new information about weak crowder−protein interactions and facilitated observation of hard particle volume exclusion and confinement in the same experimental system.

MATERIALS AND METHODS

PVP Characterization. PVP-10, -29, -40, and -55 (Fisher or Sigma) were used without purification. For light scattering experiments, a solution containing 8 mg/mL PVP in 50 mM sodium acetate buffer (pH 5.4) was prepared. A 100 μL sample of this solution was injected onto a size exclusion column (Superdex 200 10/300 GL, GE Healthcare) connected to an AKTA FPLC system (GE Healthcare) in tandem with a light scattering system. The system comprises a DAWN-EOS unit with a QELS attachment (Wyatt Technologies) and an Optilab DSP (Wyatt) for refractive index measurements. Prior to injection, the column was equilibrated with 50 mM sodium acetate buffer (pH 5.4) containing 0.02% NaN_3. Data were analyzed with *ASTRA* (Wyatt). Analysis of the data yields values for the weight-average molecular weight ($\bar{M}_W$), the number-average molecular weight ($\bar{M}_N$), the polydispersity ($\bar{M}_W/\bar{M}_N$), and the hydrated radius (R_H). The radius of gyration (R_G) is equal to $1.5R_H$ (*22*). Calculations of c^*

were made by using $\bar{M}_W$, R_G, and the equation (*22*)

$$c^* = \frac{\bar{M}_W}{{R_G}^3 N_A}$$

where N_A is Avogadro's number.

To determine partial specific volumes ($\bar{\nu}_2$), PVP samples were dried at 37 °C for 72 h and dissolved in distilled, deionized water to the desired weight concentration. The density of each solution was measured by using an Anton Paar DMA 5000 density meter. Experiments were performed in triplicate. A linear relation between the weight fraction and inverse density was used to obtain $\bar{\nu}_2$ (*36*).

Protein Expression and Purification. The plasmid containing the I29A/I37H variant of CI2 is described by Charlton et al. (*16*). The variant protein was prepared as described, with minor alterations. The single colony picked from an agar plate was transferred into a 250 mL baffled flask containing 100 mL of ^{15}N-enriched Spectra 9 medium (Cambridge Stable Isotopes). The culture in the 6 L flask was induced when the absorbance at 600 nm reached 0.8. The centrifuged lysate was treated with streptomycin sulfate (0.01 g/mL, final concentration) instead of polyethyleneimine. Size exclusion chromatography was always used, and the purified protein from anion exchange chromatography was dialyzed overnight against H_2O prior to being loaded onto the Superdex 75 column.

NMR. Amide proton exchange experiments were performed as described by Miklos et al. (*12*) on a 500 MHz spectrometer with a cold probe (Varian) at a ^{1}H sweep width of 8401.6 Hz and a ^{15}N sweep width of 2200 Hz. Buffers containing 50 mM acetate were used. We limited the ionic strength of the sample to take full advantage of the cold probe (*37*). Processing was performed with nmrPipe (*38*). Assignments have been described previously (*16*). Cross-peak volumes were quantified, plotted versus time, and fitted to exponential decays by using NMRViewJ (*39*). Examples of such curves can be seen in Figure 1 of ref *16*.

Values for k_{int} were determined as described by Hwang et al. (*40*) for 1 mM I29A/I37H variant in 50 mM sodium acetate buffer (pH 5.4, 37 °C) containing 0 and 300 g/L PVP-40. Experiments were performed on a 600 MHz spectrometer (Varian) at a ^{1}H sweep width of 10000 Hz and a ^{15}N sweep width of 2000 Hz. The water signal remained constant with mixing times from 0 to 53 ms. $R_{1B,app}$ was therefore set at 0.01 s^{-1}. As expected (*41*), the value of $R_{1B,app}$ did not alter the results.

NOESY-detected amide proton exchange experiments were performed as described by Miklos et al. (*12*) on the 500 MHz spectrometer at a ^{1}H sweep width of 8401.6 Hz. The sample comprised 1 mM I29A/I37H variant in 50 mM sodium acetate buffer (pH 5.4, 37 °C) with 50 g/L PVP-10. Processing and exponential decay fitting were performed as described for the exchange experiments, but assignments were made by matching amide−amide cross-peaks to ^{1}H shifts from the HSQC assignment corresponding to pairs of proximal amide protons.

R_1R_2 data were acquired and processed as described by Li and Pielak (*28*).

Samples for determining chemical shift changes comprised 1 mM I29A/I37H variant in 50 mM sodium acetate buffer (pH 5.4, 37 °C) with 15% D_2O and either 10 or 100 g/L PVP-55. One HSQC spectrum was acquired for each sample. The data were processed with nmrPipe. Peaks were picked with NMRViewJ and compared to the values from Charlton et al. (*16*). The chemical shift changes (δ_{av}) were calculated with the equation (*42*)

$$\delta_{av} = \left[(\Delta^1\mathrm{Hppm})^2 + \frac{(\Delta^{15}\mathrm{Nppm} \times 0.154)^2}{2}\right]^{1/2}$$

Table 2: k_{obs} Values from NOESY-Detected Amide Proton Exchange and HSQC-Detected Amide Proton Exchange in 50 g/L PVP-10 and 50 mM Sodium Acetate Buffer at pH 5.4 and 37 °C

residue(s)	k_{obs} from NOESY ($\times 10^5$ s^{-1})	k_{obs} from HSQC ($\times 10^5$ s^{-1})
Leu8	4.6	3.7
Val9	3.8	3.0
Leu8 + Val9[a]	8.4	6.7
Leu8, Val9[b]	7.0	—
Ala58	5.3	4.1
Glu59	5.5	4.6
Ala58 + Glu59[a]	10.8	8.7
Ala58, Glu59[b]	8.5	—

[a]Sum of values from individual cross-peak decays. [b]Exchange rate of the amide−amide NOESY cross-peak.

RESULTS

PVP Characterization. Light scattering and density measurements were used to quantify the properties of the polydisperse PVP samples. We performed this analysis for two reasons. First, we wanted to ensure that $\bar{M}_W$ values provided by the manufacturer were correct. Second, we wanted to ensure that our samples did not have excessive amounts of the low-molecular weight polymer. Values for $\bar{M}_W$, $\bar{M}_N$, polydispersity, R_H, the partial specific volume ($\bar{\nu}_2$), and c^* were determined (Table 1). Experiments yielded linear fits for $\bar{\nu}_2$ with R^2 values of > 0.997. A comparison of our values to results for 10 kDa PVP (*36*) indicates that our $\bar{\nu}_2$ values are accurate to three decimal places. Analysis of other PVP sizes yields a similar precision.

Stability under Crowded Conditions. ΔG^{0*}_{op} values were determined in triplicate for 33 CI2 residues under 13 conditions (0, 100, 200, and 300 g/L solutions of PVP-10, -29, -40, and -55). One experiment was also performed in 50 g/L PVP-10. A total of 1339 ΔG^{0*}_{op} values were obtained, resulting in 430 average ΔG^{0*}_{op} values. Tables of all average ΔG^{0*}_{op} values are available as Supporting Information. For comparison, Charlton et al. analyzed results from 170 ΔG^{0*}_{op} values and 34 average ΔG^{0*}_{op} values with only PVP-40 (*16*). In PVP solutions, almost all residues exhibit an increase in ΔG^{0*}_{op} compared to dilute solution. The exceptions are ΔG^{0*}_{op} values that are the same in the presence and absence of PVP.

We confirmed our conclusions from ref *16* that $k_{cl} \gg k_{int}$ [i.e., exchange occurs in the EX2 regime (*35*, *43*)] and that PVP does not affect k_{int}. We confirmed that $k_{cl} \gg k_{int}$ by performing a NOESY-HEX experiment in 50 g/L PVP-10 (*12*, *44*), a separate technique from the pH dependence of exchange in 300 g/L PVP-40 performed by Charlton et al. (*16*). The NOESY-HEX data show that the k_{obs} value for the combined amide−amide decay matches the sum of the individual decays (Table 2), which is expected when $k_{cl} \gg k_{int}$ (*12*). To determine k_{int}, we repeated the CLEANEX-PM experiments in 0 and 300 g/L PVP-40 (*16*). For the fully exposed loop residue His37, k_{int} was the same in 300 g/L PVP-40 and in dilute solution (Figure S1 of the Supporting Information). The CLEANEX-PM results also confirm that the activity of water is not changed between dilute solution and crowded conditions, because k_{int} depends on water activity (*8*).

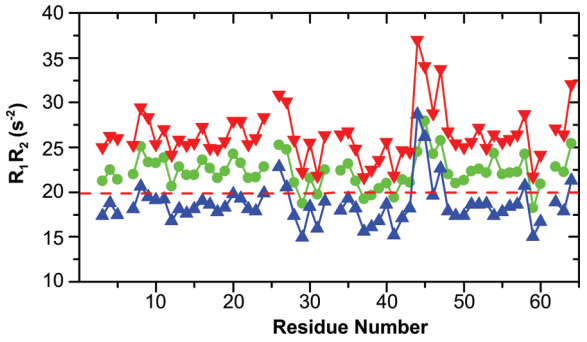

FIGURE 3: Histogram of R_1R_2 values for 0.4 mM CI2 (200 mM sodium acetate at pH 5.4 and 25 °C) with 100 g/L PVP-40 (blue), 200 g/L PVP-40 (green), and 200 g/L BSA (red). The rigid limit is depicted as a dashed red line. The rigid limit value and data for 200 g/L BSA are from Li and Pielak (*28*).

Trends in stability were defined by linearly regressing plots of ΔG_{op}^{0*} versus either PVP molecular weight or PVP concentration for each of the 33 residues for which we could obtain exchange rates. The sign of the slopes indicated the presence or absence of trend. First, we examined trends arising from PVP molecular weight. For 100 g/L solutions of PVP, the mean slope for all observable residues was -3.0 ± 0.8 cal mol^{-1} kDa^{-1}, indicating the presence of a trend. For 200 and 300 g/L solutions of PVP, the mean slopes were 0.9 ± 0.7 and 1 ± 2 cal mol^{-1} kDa^{-1}, respectively. These two results indicate the absence of a trend at higher PVP concentrations. Concentration dependence also yielded trends.

In all concentration-dependent trends, a positive correlation was noted between PVP concentration and CI2 stability. Upon examination of results for individual residues, the trend was refined into three types. Figure 2 depicts an example of each trend using data from one representative backbone amide: Ile20 (in the α-helix), Asn56 (in a turn), and Trp5 (at the end of a short β-sheet). All three residues report an increase in stability from 0 to 100 g/L PVP. Ile20 shows the most pronounced increase with an increase in PVP concentration. We call this trend "volume exclusion". Asn56 exhibits no further stabilization with an increase in PVP concentration. We call this trend "native-state binding". Trp5 shows some additional increase as the PVP concentration is increased from 200 to 300 g/L. We call this trend the "mixed effect". The behaviors of these three residues were used to bin the other residues for which stability data were obtained. Figure 2 also shows the backbone of the protein colored to indicate residues following each trend. We used R_1R_2 values and chemical shift changes to investigate soft interactions.

Soft Interactions. The variety of trends prompted us to probe soft interactions between PVP and CI2. R_1R_2 values were measured for backbone amide ^{15}N atoms of CI2 in solutions containing 100, 200, and 300 g/L PVP-40 at pH 5.4 and 25 °C. CI2 has a correlation time of >6 ns under all these conditions because of the enhanced viscosity of the PVP solutions. A histogram of the results for 100 and 200 g/L PVP is shown in Figure 3. Note that 200 g/L PVP results in smaller R_1R_2 values compared to those acquired in 200 g/L BSA (*28*). R_1R_2 values acquired in 300 g/L PVP cannot be compared to BSA results, because line broadening obviates the acquisition of R_2 values in 300 g/L BSA. These data were corroborated by examination of changes in chemical shift.

In a 10 g/L solution of PVP-55 at pH 5.4 and 37 °C, chemical shift changes, compared to dilute solution (Figure 4), are smaller

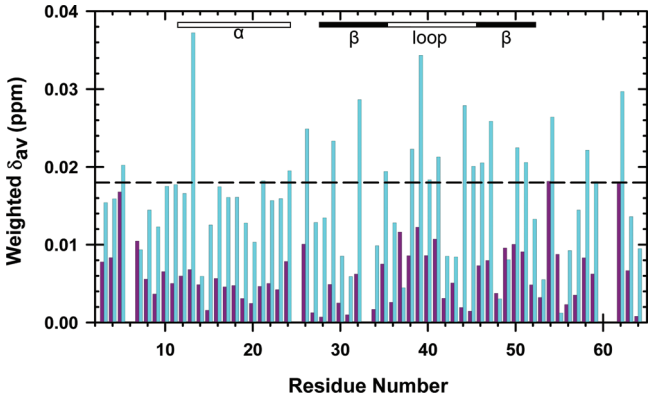

FIGURE 4: Histogram of changes in backbone ^{15}N and ^{1}H chemical shifts for 1 mM CI2 upon addition of 10 g/L PVP-55 (purple) and 100 g/L PVP-55 (cyan) in 50 mM sodium acetate buffer at pH 5.4 and 37 °C. Elements of secondary structure are indicated above the histogram. Values above the horizontal dashed line, as defined by Charlton et al. (*16*), represent statistically significant changes in chemical shift.

than what we can measure (*16*). At 100 g/L, however, several significant changes are noted. The regions in which changes occur include the loop (Gly35−Ile44), the second β-sheet (Asp45−Asp52), and turns (Figure 4). The implications of these data are addressed below.

DISCUSSION

PVP Crowding Trends. Volume exclusion theory predicts that crowding will increase stability if the crowder's size is close to that of the protein (*45*). Our observations are consistent with this prediction because PVP increases CI2 stability under all conditions (Figure 2). Given the polydispersity of PVP, we believe these values underestimate the effect of volume exclusion, because the results are more heavily influenced by short polymers present in the mixture. In addition, our residue-level interrogation yields stability trends as a function of PVP molecular weight and concentration (Figure 2).

Molecular Weight Trends. As mentioned in the introductory section, there are two volume exclusion regimes: hard particle exclusion and confinement (*17*, *20*). Above a certain polymer concentration, known as c^*, synthetic polymers begin to form a network, leading to a transition from individual, independently moving molecules (dilute) to a mixture of entangled polymers (semidilute) (*22*). Our calculations for PVP indicate that the transition occurs at concentrations of >100 g/L (Table 1). When solution conditions change from dilute to semidilute (i.e., PVP concentration is above c^*), so does the model for volume exclusion. The change helps inform our interpretation of the molecular weight dependence.

The change from the dilute to the semidilute regime is accompanied by a change in theoretical parameters, which are affected by crowder concentration and molecular weight in different ways. For hard particle exclusion, the key parameters are sphere size and number density. These parameters correspond to our experimental variables, molecular weight, and concentration. The relationship between PVP particle size and molecular weight is consistent with a self-avoiding walk polymer (*22*), and as the weight concentration increases, so does the number density.

The results from 100 g/L PVP are consistent with hard particle exclusion because they are consistent with predictions of stability changes based on the size of independent hard sphere crowders.

Specifically, ΔG_{op}^{0*} increases with an increase in PVP concentration, but higher-molecular weight PVPs have a weaker stabilizing effect (*21*). The data for 200 and 300 g/L PVP solutions are more consistent with confinement.

For confinement, the shape and size of the confining space should be independent of PVP molecular weight. At concentrations at which PVP molecules are entangled, changing the molecular weight of PVP should not change the confining space. Our observations point to confinement as a more appropriate model for 200 and 300 g/L PVP solutions, because there is no consistent molecular weight dependence. Increasing the concentration, however, should decrease the average size of the confining space. As the space shrinks, protein stability should increase. This matches our results from experiments in 200 and 300 g/L PVP, because stability increases with an increase in PVP concentration. In summary, the transition from the dilute to an entangled regime of the polymer solution is accompanied by a change in the model for crowding, from hard particle volume exclusion to confinement. Concentration trends yielded results that indicated both volume exclusion effects and soft interactions between the protein and crowder.

Concentration Trends. Stabilization by volume exclusion is expected to show a strong, consistent increase with crowding agent concentration, as shown by Leu8, Val9, Lys11, Val19, Leu21, Gln28, Ile30, Leu32, Val47, Leu49, Phe50, Val51, Ile57, Ala58, Glu59, and the exemplar, Ile20 (Figure 2). The $\Delta\Delta G_{op}^{0*}$ values for these residues fall between 0.9 and 3.0 kcal/mol in 300 g/L PVP, which is also consistent with predictions for the magnitude of volume exclusion effects (*46*).

With the exception of Val9, residues in the volume exclusion regime either are involved in global unfolding or are backbone hydrogen bond partners of global unfolders (*30*). This result is expected, because volume exclusion increases protein stability through destabilization of the denatured ensemble. For residues on the global path, the exchange-competent unfolded states are most destabilized by volume exclusion, because the globally unfolded state creates the largest change in covolume. These results indicate a contribution to stability purely associated with volume exclusion. Some residues, as shown by Asn56 (Figure 2), indicated native-state binding trends that could not be explained with traditional exclusion models.

Native-state binding is expected to exhibit saturation behavior. That is, an increase in stability is noted at lower PVP concentrations, with no increase upon further addition of PVP. This trend is exhibited by Val13, Asp55, Asn56, Arg62, Val63, and Gly64. These residues and those nearby in the primary structure also exhibit chemical shift changes (Val13, Leu54, and Arg62) and increased R_1R_2 values [Lys11, Glu15, Leu54, Asp55, Asn56, and Gly64 (Figure 3)], supporting the idea that native-state PVP binding plays a role in effecting stability. Consistent with the idea of weak binding, these effects seem to be absent at the lowest PVP concentrations, because no significant chemical shift changes were noted in solutions containing 55 kDa PVP at 10 g/L (Figure 4). Further implications of weak native-state binding are discussed in the next section.

These data point to weak native-state binding as the cause of this stability trend. Native-state binding, however, differs from another stabilizing soft interaction, the solvophobic effect (*47*). This effect, as exemplified by TMAO and other osmolytes, continuously increases protein stability with an increasing cosolute concentration. PVP, however, shows saturation. This set of residues does not show a dependence of ΔG_{op}^{0*} on PVP concentration, ruling out the solvophobic effect as a source of the stability increase. The lack of PVP concentration dependence also rules out volume exclusion as a source of stabilization. We rationalize the lack of an excluded volume effect on the basis of the fact that nearly all of these residues are surface-exposed and would have exchange-accessible states that require minimal rearrangement of the protein. As such, the minor change in the size of the protein from the closed to open state for these residues would lead to a minimal contribution from volume exclusion. All other residues exhibit properties of both binding and volume exclusion. We call this trend, as represented by Leu49 (Figure 2), the mixed effect.

The mixed effect combines weak native-state binding with volume exclusion. A modest increase in stability is noted at lower crowder concentrations, with a plateau in stability that is only slightly surpassed in 300 g/L PVP. The majority of residues not implicated in global unfolding fall into this bin (Trp5, Gly10, Ala16, Lys17, Lys18, Gln22, Lys24, Val34, Arg46, Arg48, and Asp52). For the mixed effect, it is likely that weak native-state binding dominates the stabilizing effect of PVP at low concentrations. At higher concentrations, the roles are reversed, and volume exclusion becomes more important.

In summary, we find evidence of two types of interactions, volume exclusion and binding. Volume exclusion affects ~80% of the residues studied, while binding affects ~50% of the residues. The fact that 80% of residues show effects from volume exclusion is expected; volume exclusion should affect all residues, albeit to different extents. Binding affects 50% of the residues, yet this important effect is neglected in many studies of crowding. To investigate these weak binding effects further, R_1R_2 values were used.

Soft Interactions. Large R_1R_2 values, indicative of binding (*28*), can result from strong and weak soft interactions. We ruled out strong PVP−CI2 interactions because CI2 cross-peaks are not drastically broadened by PVP (*16*). Backbone amide nitrogens from a "pure" species (i.e., 100% monomer, 100% dimer, etc.) that does not exhibit conformation exchange should have R_1R_2 values below a threshold known as the rigid limit line (*28*). Mixtures yield larger values. The value for the rigid limit is approximately 20 s^{-2} for data acquired on a 600 MHz NMR spectrometer. We need only consider binding interactions involving monomers and dimers of CI2 for three reasons. First, Charlton et al. (*16*) used NMR-detected diffusion experiments to show that CI2 forms no more than a dimer in a 300 g/L solution of PVP-40 at pH 5.4 and 37 °C. Second, CI2 does not undergo significant conformation exchange in dilute solution (*28*). Third, PVP decreases the amide proton exchange rate. This decrease in rate is only consistent with the absence of PVP-induced conformation exchange because an increase in the level of conformation exchange would increase the level of amide proton exchange.

In a 300 g/L PVP-40 solution, the average R_1R_2 value (26 s^{-2}) is essentially equal to the maximum theoretical value for a mixture of CI2 monomers and dimers (25 s^{-2}) (*28*). Taken together with the fact that this theoretical maximum only occurs at 50% homodimer formation and the conclusions of Charlton et al. (*16*), this observation indicates that although limited CI2 self-association may occur, there are also weak soft interactions between PVP and CI2. Our chemical shift analysis corroborates this information.

Chemical shift changes arise from changes in native-state chemical environment. This environmental effect could arise from PVP binding or PVP-induced conformational changes.

Shift changes occur at PVP concentrations of ≥100 g/L in tightly packed regions, including the second β-sheet (Asp45−Asp52). This observation leads us to invoke weak chemical interactions between PVP and the native state of CI2 as the cause of the chemical shift changes, because tightly packed regions are unlikely to undergo significant conformational changes. These weak native-state interactions, which account for the binding trend that stabilizes 50% of the residues studied, are distinct from nonspecific interactions, which are destabilizing.

Nonspecific interactions will destabilize proteins, as is the case with urea (*24*). It was noted by Charlton et al. that the monomer model of PVP, *N*-ethylpyrrolidone, destabilizes CI2 (*16*). This type of interaction is expected to persist in the polymer, although it should be attenuated because the polymer partially excludes access. The increase in R_1R_2 with an increase in PVP concentration (Figure 3) is evidence of the persistence of nonspecific chemical interactions between the crowder and the protein. The weak destabilizing interaction mitigates the stabilizing effects in our system, resulting in an underestimate of contributions from volume exclusion and native-state binding interactions. The contribution of nonspecific interactions may be large in our experiments because of the low ionic strength used. Electrostatics should not be a major contributor, however, as PVP is uncharged. Proteins do, however, have electrostatic effects. As shown in Figure 3, the interactions of CI2 with PVP are weaker than interactions with bovine serum albumin (BSA). We expect nonspecific binding to have a stronger effect when proteins are used as crowders as opposed to synthetic polymers because of the increase in the number of nonspecific interactions (*32*).

Summary and Concluding Remarks. We quantified both the effect of PVP molecular weight and concentration. Consistent with volume exclusion models, PVP never destabilizes the protein. We observe two trends for the molecular weight dependence and three trends for the concentration dependence. The molecular weight trends can be explained by the two regimes of volume exclusion, hard particle exclusion and confinement. The concentration dependence can be explained by two types of interactions, volume exclusion and soft interactions.

Our study of molecular weight dependence on protein stability yielded two trends corresponding to two models of volume exclusion. At low PVP concentrations, there is a diminution in the stabilization effect with an increase in molecular weight, as expected from hard sphere volume exclusion. At higher concentrations, there is no molecular weight dependence, signaling a shift from hard particle volume exclusion to confinement as the polymer becomes entangled. Concentration trends yielded contributions from both volume exclusion and weak native-state interactions.

Volume exclusion explains the concentration-dependent interaction for most of the globally unfolding residues. However, native-state binding is present for other residues for which ΔG_{op}^{0*} increases at lower concentrations without a further increase at higher concentrations. Many residues exhibit effects from both volume exclusion and binding. Binding was investigated independently, and our results uncover soft interactions between PVP and CI2.

Our most surprising conclusion is that soft interactions between the crowding agent and the native state of the protein play such a large role despite the fact that we purposely chose a system that minimizes soft interactions (*32*). Weak nonspecific interactions mitigate the effects of volume exclusion, indicating that our analysis underestimates the effect of volume exclusion. We also find evidence of native-state interactions. Specifically, 50% of the residues show effects from weak native-state interactions. We expect soft interactions to play an even larger role in biological systems, where proteins are crowded by other proteins, which can have stabilizing or destabilizing soft interactions. In some cases, destabilizing nonspecific interactions could compete with the stabilizing volume exclusion effect. Such soft interactions will need to be addressed to understand the full effects of crowding in cells. In summary, although macromolecular crowding is often discussed solely in the context of volume exclusion, studies must be expanded to include soft interactions.

ACKNOWLEDGMENT

We thank Greg Young of the University of North Carolina Biomolecular NMR Facility and Ashutosh Tripathy of the University of North Carolina Macromolecular Interactions Facility for assistance and Elizabeth Pielak for helpful comments.

SUPPORTING INFORMATION AVAILABLE

Tables containing average ΔG_{op}^{0*} values with standard errors and k_{int} values for CI2 under experimental conditions and figures of a CLEANEX-PM buildup curve and exchange curves for 300 g/L PVP-10. This material is available free of charge via the Internet at http://pubs.acs.org.

REFERENCES

1. Capp, M. W., Cayley, D. S., Zhang, W. T., Guttman, H. J., Melcher, S. E., Saecker, R. M., Anderson, C. F., and Record, M. T. (1996) Compensating effects of opposing changes in putrescine (2^+) and K^+ concentrations on *lac* repressor-*lac* operator binding: *In vitro* thermodynamic analysis and *in vivo* relevance. *J. Mol. Biol. 258*, 25–36.
2. Dedmon, M. M., Patel, C. N., Young, G. B., and Pielak, G. J. (2002) FlgM gains structure in living cells. *Proc. Natl. Acad. Sci. U.S.A. 99*, 12681–12684.
3. Ignatova, Z., and Gierasch, L. M. (2004) Monitoring protein stability and aggregation *in vivo* by real-time fluorescent labeling. *Proc. Natl. Acad. Sci. U.S.A. 101*, 523–528.
4. McGuffee, S. R., and Elcock, A. H. (2010) Diffusion, crowding & protein stability in a dynamic molecular model of the bacterial cytoplasm. *PLoS Comput. Biol. 6*, e1000694.
5. Elcock, A. H. (2010) Models of macromolecular crowding effects and the need for quantitative comparisons with experiment. *Curr. Opin. Struct. Biol. 20*, 196–206.
6. Lumry, R., Biltonen, R., and Brandts, J. F. (1966) Validity of the "two-state" hypothesis for conformational transitions of proteins. *Biopolymers 4*, 917–944.
7. Clarke, J., and Itzhaki, L. S. (1998) Hydrogen exchange and protein folding. *Curr. Opin. Struct. Biol. 8*, 112–118.
8. Englander, S. W., and Kallenbach, N. R. (1983) Hydrogen exchange and structural dynamics of proteins and nucleic acids. *Q. Rev. Biophys. 16*, 521–655.
9. Bodenhausen, G., and Ruben, D. J. (1980) Natural abundance nitrogen-15 NMR by enhanced heteronuclear spectroscopy. *Chem. Phys. Lett. 69*, 185–189.
10. Kay, L., Keifer, P., and Saarinen, T. (1992) Pure absorption gradient enhanced heteronuclear single quantum correlation spectroscopy with improved sensitivity. *J. Am. Chem. Soc. 114*, 10663–10665.
11. Hammes, G. G., Chang, Y. C., and Oas, T. G. (2009) Conformational selection or induced fit: A flux description of reaction mechanism. *Proc. Natl. Acad. Sci. U.S.A. 106*, 13737–13741.
12. Miklos, A. C., Li, C., and Pielak, G. J. (2009) Using NMR-detected backbone amide ^1H exchange to assess macromolecular crowding effects on globular-protein stability. *Methods Enzymol. 466*, 1–18.
13. Linderstrøm-Lang, K. U. (1958) Deuterium exchange and protein structure. In Symposium on Protein Structure (Neuberger, A., Ed.), pp 23−34, Methuen, London.
14. Bai, Y., Milne, J. S., Mayne, L., and Englander, S. W. (1993) Primary structure effects on peptide group hydrogen exchange. *Proteins: Struct., Funct., Genet. 17*, 75–86.

15. Zhang, Y.-Z. (1995) Protein and peptide structure and interactions studied by hydrogen exchange and NMR. Ph.D. Thesis, Structural Biology and Molecular Biophysics, University of Pennsylvania, Philadelphia.
16. Charlton, L. M., Barnes, C. O., Li, C., Orans, J., Young, G. B., and Pielak, G. J. (2008) Macromolecular crowding effects on protein stability at the residue level. *J. Am. Chem. Soc. 130*, 6826–6830.
17. Zhou, H. X., Rivas, G. N., and Minton, A. P. (2008) Macromolecular crowding and confinement: Biochemical, biophysical, and potential physiological consequences. *Annu. Rev. Biophys. 37*, 375–397.
18. Davis-Searles, P. R., Saunders, A. J., Erie, D. A., Winzor, D. J., and Pielak, G. J. (2001) Interpreting the effects of small uncharged solutes on protein-folding equilibria. *Annu. Rev. Biophys. Biomol. Struct. 30*, 271–306.
19. Miller, W. G., and Goebel, C. V. (1968) Dimensions of protein random coils. *Biochemistry 7*, 3925–3935.
20. Zhou, H. X., and Dill, K. A. (2001) Stabilization of proteins in confined spaces. *Biochemistry 40*, 11289–11293.
21. Minton, A. P. (1983) The effect of volume occupancy upon the thermodynamic activity of protein: Some biochemical consequences. *Mol. Cell. Biochem. 55*, 119–140.
22. Rubinstein, M., and Colby, R. (2003) Polymer Physics, Oxford University Press, New York.
23. Timasheff, S. N. (2002) Protein-solvent preferential interactions, protein hydration, and the modulation of biochemical reactions by solvent components. *Proc. Natl. Acad. Sci. U.S.A. 99*, 9721–9726.
24. Lim, W. K., Rösgenc, J., and Englander, S. W. (2009) Urea, but not guanidinium, destabilizes proteins by forming hydrogen bonds to the peptide group. *Proc. Natl. Acad. Sci. U.S.A. 106*, 2595–2600.
25. Vicky, D.-N., and Loria, J. P. (2007) The effects of cosolutes on protein dynamics: The reversal of denaturant-induced protein fluctuations by trimethylamine *N*-oxide. *Protein Sci. 16*, 20–29.
26. Isom, D. G., Vardy, E., Oas, T. G., and Hellinga, H. W. (2010) Picomole-scale characterization of protein stability and function by quantitative cysteine reactivity. *Proc. Natl. Acad. Sci. U.S.A. 107*, 4908–4913.
27. Kneller, J. M., Lu, M., and Bracken, C. (2002) An effective method for the discrimination of motional anisotropy and chemical exchange. *J. Am. Chem. Soc. 124*, 1852–1853.
28. Li, C., and Pielak, G. J. (2009) Using NMR to distinguish viscosity effects from nonspecific protein binding under crowded conditions. *J. Am. Chem. Soc. 131*, 1368–1369.
29. Jackson, S. E., and Fersht, A. R. (1991) Folding of chymotrypsin inhibitor 2. 1. Evidence for a two-state transition. *Biochemistry 30*, 10428–10435.
30. Neira, J. L., Itzhaki, L. S., Otzen, D. E., Davis, B., and Fersht, A. R. (1997) Hydrogen exchange in chymotrypsin inhibitor 2 probed by mutagenesis. *J. Mol. Biol. 270*, 99–110.
31. Molyneux, P. (1983) Water-soluble synthetic polymers: Properties and behavior, Vol. 1, CRC Press, Boca Raton, FL.
32. Wang, Y., Li, C., and Pielak, G. J. (2010) Effects of proteins on protein diffusion. *J. Am. Chem. Soc. 132*, 9392–9397.
33. Ladurner, A. G., and Fersht, A. R. (1999) Upper limit of the time scale for diffusion and chain collapse in chymotrypsin inhibitor 2. *Nat. Struct. Mol. Biol. 6*, 28–31.
34. Güven, O., and Eltan, E. (1981) Molecular association in aqueous solutions of high molecular weight poly(N-vinyl-2-pyrrolidone). *Makromol. Chem. 182*, 3129–3134.
35. Bai, Y. W., Sosnick, T. R., Mayne, L., and Englander, S. W. (1995) Protein folding intermediates: Native-state hydrogen exchange. *Science 269*, 192–197.
36. Sadeghi, R., and Taghi Zafarani-Moattar, M. (2004) Thermodynamics of aqueous solutions of polyvinylpyrrolidone. *J. Chem. Thermodyn. 36*, 665–670.
37. Kelly, A. E., Ou, H. D., Withers, R., and Dötsch, V. (2002) Low-conductivity buffers for high-sensitivity NMR measurements. *J. Am. Chem. Soc. 124*, 12013–12019.
38. Delaglio, F., Grzesiek, S., Vuister, G. W., Zhu, G., Pfeifer, J., and Bax, A. (1995) NMRPipe: A multidimensional spectral processing system based on UNIX pipes. *J. Biomol. NMR 6*, 277–293.
39. Johnson, B. A., and Blevins, R. A. (1994) NMR View: A computer program for the visualization and analysis of NMR data. *J. Biomol. NMR 4*, 603–614.
40. Hwang, T.-L., van Zijl, P. C. M., and Mori, S. (1998) Accurate quantitation of water-amide exchange rates using the phase-modulated CLEAN chemical EXchange (CLEANEX-PM) approach with a fast-HSQC (FHSQC) detection scheme. *J. Biomol. NMR 11*, 221–226.
41. Bertini, I., Ghosh, K., Rosato, A., and Vasos, P. R. (2003) A high-resolution NMR study of long-lived water molecules in both oxidation states of a minimal cytochrome *c*. *Biochemistry 42*, 3457–3463.
42. Davison, T. S., Nie, X., Ma, W., Lin, Y., Kay, C., Benchimol, S., and Arrowsmith, C. H. (2001) Structure and functionality of a designed p53 dimer. *J. Mol. Biol. 307*, 605–617.
43. Frost, A. A., and Pearson, R. G. (1953) Kinetics and Mechanism, John Wiley & Sons, New York.
44. Wagner, G. (1980) A novel application of nuclear Overhauser enhancement (NOE) in proteins: Analysis of correlated events in the exchange of internal labile protons. *Biochem. Biophys. Res. Commun. 97*, 614–620.
45. Zhou, H. X. (2008) Effect of mixed macromolecular crowding agents on protein folding. *Proteins: Struct., Funct., Bioinf. 72*, 1109–1113.
46. Minton, A. P. (2000) Effect of a concentrated "inert" macromolecular cosolute on the stability of a globular protein with respect to denaturation by heat and by chaotropes: A statistical-thermodynamic model. *Biophys. J. 78*, 101–109.
47. Auton, M., and Bolen, D. W. (2005) Predicting the energetics of osmolyte-induced protein folding/unfolding. *Proc. Natl. Acad. Sci. U.S.A. 102*, 15065–15068.
48. DeLano, W. L. (2002) The PyMOL molecular graphics system, DeLano Scientific, Palo Alto, CA.